

INVESTIGATION ON THE UNCONSTRAINED MICROFLUIDIC HEAT SINK WITH HIGH ANTI-BLOCKAGE CAPACITY FOR MULTIPLE HOTSPOTS SYSTEM

Lihang YU^{a,b}, Yuxin YE^{a,b}, Zhenyu WANG^c, Ruiwen LIU^a, Xiangbin DU^a, Yanmei KONG^a,
Shichang YUN^a, Jie WANG^{a,b}, Yulin SHI^{a,b}, Binbin JIAO^{a,*}

^a Institute of Microelectronics of the Chinese Academy of Sciences, Beijing 100029, China

^b University of Chinese Academy of Sciences, Beijing 100049, China

^c Department of Integrated Circuits and Intelligent Systems, Peking University, Beijing 100871, China

*Corresponding author; E-mail: jiaobinb@ime.ac.cn

Microfluidic heat sinks are regarded as an efficient cooling solution in microelectronic systems. However, as the hydraulic diameter of the microfluidic heat sinks shrinks, the blockage problem may occur due to the particles caused by cooling components' abrasion, which limits the application in long-term operation. This paper proposes an unconstrained microfluidic heat sink (UCMFHS) with high anti-blockage capacity for multiple hotspot systems, which aims to solve the blockage problem. The position and shape of the micro pin fins in UCMFHS are optimized by the computational fluid dynamics (CFD) model. According to the test requirements of anti-blockage capacity and cooling performance, the test platform is built, which adopts the thermal test chips (TTCs) as heat source array. The results show that when the coolant particle concentration is 0.5%, the pressure drop variation is less than 0.3 kPa in UCMFHS, which is 99.43% lower than the control sample. The average temperature and temperature non-uniformity coefficient of 16 hotspots under the condition of 1200 W/cm² and 125 mL/min are 141.1 °C and 0.049, respectively. Therefore, the UCMFHS has both anti-blockage capacity and cooling capacity and is considered to have a high application prospect in long-term multi-hotspot cooling.

Keywords: *Unconstrained microfluidic heat sink; Anti-blockage capacity; Temperature uniformity; Pin fins; Long-term operation; Multi-hotspots cooling*

1. Introduction

With the development of integration and miniaturization, more and more functional components are integrated in the electronic system, which leads to a sharp increase in the heat flux density in the system [1, 2]. The high temperature will threaten the reliability and performance of the components in the system [3]. Therefore, it is necessary to design an efficient and reliable cooling method to ensure the system's proper operation [4]. The concept of the microfluidic heat sink was first proposed by Tuckerman and Pease in 1981 [5]. Due to the excellent heat dissipation capacity [6], the microfluidic heat sink is widely used in the cooling of microelectronic systems [7-14].

The abrasion of the cooling components may generate particles, which deposit continually in the microfluidic structure during the long-term operation [15]. As the hydraulic diameter of the microfluidic structure shrinks, the blockage problem happens as the aggregate size is comparable to the microfluidic structure size [16-19], which is on the order of microns [20]. The blockage problem will affect the flow state of the coolant [21], which influences the cooling performance of the microfluidic heat sink. In more serious cases, the critical paths of the microfluidic structure are blocked, resulting in the failure of the microfluidic heat sink to work properly [22]. The blockage problem seriously affects the reliability and service life of the microfluidic heat sink. Therefore, a microfluidic heat sink with good anti-blockage capacity and cooling capacity is of great significance. Many researches have been conducted to solve the blockage problem in microfluidic structures. Optimizing the microfluidic structure, which makes the microfluidic heat sink unaffected by the blockage, is one of the common ways to solve the blockage problem of microfluidic structure. Pejman et al. [23] introduced a systematic approach for Hybrid Topology/Shape (HyTopS) optimization. The proposed HyTopS optimization scheme added redundant structures to the topological network of microfluidic structures to improve the anti-blockage capacity. Pety et al. [24] designed redundant cooling networks, which provided sufficient cooling capacity when the microfluidic structure was partially blocked. The temperature rise at single blockage conditions was reduced from 35°C to 7°C according to the simulation results. Wang et al. [25] designed a bionic tree-shaped microfluidic structure. The simulation study showed that when the microfluidic structure was partially blocked, the cooling performance of the microfluidic heat sink was not affected [26]. The results show that such a microfluidic structure had better stability in case of accidental blockage. The tree-like microfluidic structure with loops [27] can further increase the anti-blockage capacity of the microfluidic heat sink. The branching level can decrease the temperature gradient and pressure drop when the blockage occurs.

For improving the cooling performance of the heat sink, the local channel densities can be tuned to solve the temperature non-uniformity problem. Wu et al. [28] optimized the local channel widths by genetic algorithm and reduced the maximum junction surface temperature difference from 45 °C to 13 °C at a heat flux density of 200 W/cm². Designing novel microfluidic structures is also a useful method to enhance thermal performance. Riera et al. [29] proposed stepwise varying width microchannel and the temperature standard deviation was found to be 0.8 when the cooling scheme was used. Ansari et al. [30] proposed microchannel-pin fin hybrid heat sink, which was designed with the microchannel for low heat flux zone and micro pin fins array for high heat flux zone, and realized remarkable improvement in the cooling capacity compared to the non-hybrid heat sink. Tan et al. [31] designed a novel multi-scale leaf vein-shaped microchannel network to improve temperature uniformity for multiple hotspot systems.

The recent papers on improving the anti-blockage capacity are mainly carried out through simulation with few experiments, and few researches are about the trade-off between anti-blockage capacity and cooling performance of the microfluidic heat sink. The studies on improving cooling performance are mainly achieved by dense channel structures which reduce the anti-blockage capacity of the cooling structure. To solve these problems, the UCMFHS with high anti-blockage capacity for multiple hotspots system was proposed, which balanced anti-blockage capacity with cooling capacity. The microfluidic structure was optimized to improve the temperature uniformity of the multiple hotspots system. The optimized microfluidic structure was fabricated by deep reactive ion etching

(DRIE) and wafer bonding, and then the thermal characteristics of the microfluidic heat sink were tested by using TTC chips as the heat source array. CuO solid particles were added to the coolant, and then the change of the pressure drops in the microfluidic heat sink during the long-term operation was tested to evaluate the anti-blockage capacity.

2. The concept of the unconstrained microfluidic heat sink

Reducing the ratio of the particle diameter to the microfluidic structure diameter [18] can improve the anti-blockage capacity. Increasing the number of flow channels [23] can ensure that the microfluidic heat sink can work normally in extreme cases of partial blockage. Therefore, we designed the UCMFHS composed of micro pin fins by combining large-size flow channels with multiple flow channels.

Figure 1 shows the design of the UCMFHS. Figure 1 (a) shows the inlet and outlet design of the UCMFHS, which improves the cooling performance by adopting multiple inlets and outlets to shorten the flow length [32]. The triangular micro pin fins which have the highest heat transfer rate [33] among different geometries micro pin fins are chosen in the design, as shown in Fig. 1. (b). Figure 1 (c) and (d) show the distribution of micro pin fins. The size of the microfluidic heat sink is $50 \text{ mm} \times 50 \text{ mm} \times 1.4 \text{ mm}$, and the flow channel area is $47 \times 47 \text{ mm}^2$.

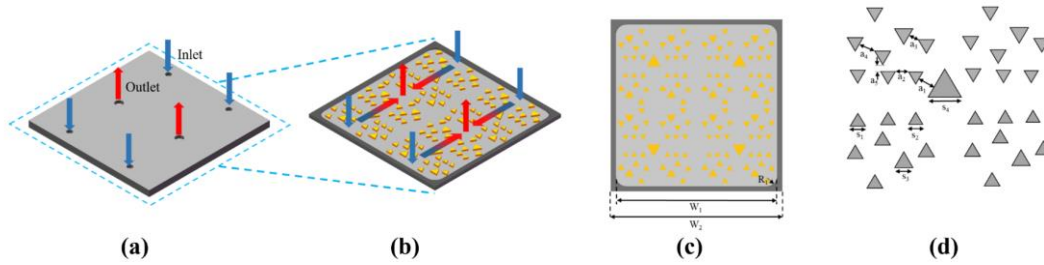


Fig. 1. (a)Schematic of the UCMFHS ;(b) Section view of the heat sink; (c)~ (d) Distribution of the micro pin fins

3. Numerical investigation

The hydraulic diameter characterizes the passage capacity of the channel. A channel with a large hydraulic diameter can make it easier for fluid to pass through which makes it difficult for blockages to occur. For channels with rectangular cross-section, the hydraulic diameter is calculated as:

$$D_H = \frac{2HW}{H+W} \quad (1)$$

where H and W are the height and width of the channel cross-section, respectively. Therefore, the anti-blockage capacity can be improved by large channel width, which is achieved by the large spacing of micro pin fins. However, the increased spacing of the micro pin fins in the UCMFHS will influence the cooling performance [34]. So, the design of the UCMFHS is optimized to enhance the cooling performance while maintaining good anti-blockage capacity.

3.1. CFD model

The UCMFHS consists of silicon pin fins. The heat source consists of 16 silicon rectangular squares with a width of 1 mm and length of 1 mm. The top surface of squares is supplied with a heat

flux of 400-2000 W/cm². The coolant is deionized water and the flow rate is set to 25-200 mL/min. To simulate the actual working conditions, the Au80-Sn20 solder interface material between the UCMFHS and the heat source is equivalent to a thin-layer thermal resistance with a thickness of 100 μm and thermal conductivity of 30 Wm⁻¹K⁻¹. The UCMFHS is symmetrical and therefore the temperature field will have the same symmetry. To reduce the computational complexity of the simulation, only half of the model is simulated in this study, as shown in Fig. 2.

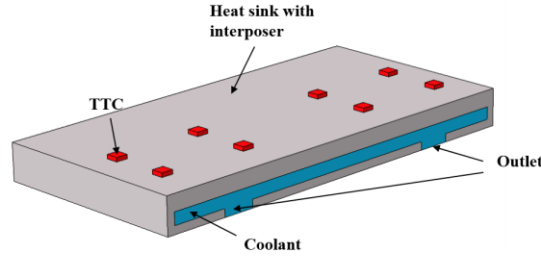


Fig. 2. Schematic diagram of the simulation model

Besides, some assumptions in the calculation are as follows:

- (1) The calculated Reynolds number $Re < 2000$ which indicates the fluid is laminar; And the fluid is incompressible.
- (2) The flow characteristics still obey the N-S equation and the continuum hypothesis when the Reynolds number is less than 2000 [35].
- (3) The radiative heat transfer is negligible.
- (4) The Reynolds number is not high in the study, so a steady-state condition is considered.
- (5) The effect of the thermal interface material is equivalent to the thin layer thermal resistance.
- (6) The liquid is considered under single phase flow.

The governing equations of the flow and the heat transfer are as follows.

Continuity equation:

$$\nabla(\rho \vec{u}) = 0 \quad (2)$$

where ρ is the fluid density, \vec{u} is the velocity vector.

Momentum equation:

$$\rho \nabla(\vec{u} \cdot \nabla) \vec{u} = \nabla \cdot [-p \mathbf{I} + \boldsymbol{\tau}] \quad (3)$$

$$\boldsymbol{\tau} = \mu \left(\nabla \vec{u} + (\nabla \vec{u})^T \right) \quad (4)$$

where p is the pressure, \mathbf{I} is the unit tensor, $\boldsymbol{\tau}$ is the viscous stress tensor, μ is the dynamic viscosity of the fluid.

Energy equation:

$$\rho c_p \vec{u} \cdot \nabla T + \nabla \cdot (-k \nabla T) = Q \quad (5)$$

where c_p is the specific heat capacity of the fluid at constant pressure, T is the temperature of the fluid, k is the thermal conductivity of the fluid, and Q is the heat source. The variations of the liquid properties over temperature are considered for precise calculation. The thermal conductivity (k) is expressed as follow:

$$k(T) = -0.869083936 + 0.00894880345 * T - 1.58366345 \times 10^{-5} * T^2 + 7.97543259 \times 10^{-9} * T^3 \quad (6)$$

The specific heat (c_p) is expressed as follow:

$$c_p(T) = 12010.1471 - 80.4072879 * T + 0.309866854 * T^2 - 5.38186884 \times 10^{-4} * T^3 + 3.62536437 \times 10^{-7} * T^4 \quad (7)$$

The density of the working fluid (ρ) is expressed as follow:

$$\rho(T) = 432.257114008512 + 4.969288832655160 * T - 0.013395065634452 * T^2 + 0.000010335053319 * T^3 \quad (8)$$

Some parameters are adopted to evaluate the cooling performance of the UCMFHS. The first parameter is the average temperature of the hotspots which is expressed as follow:

$$T_{average} = \frac{\sum_{i=1}^n T_i}{n} \quad (9)$$

Then the second parameter is the non-uniformity coefficient (NUC), which is defined as the ratio of the standard deviation of the hotspot temperatures to the average temperature of hotspots [36, 37]. The NUC is expressed as follow:

$$NUC = \frac{SDT}{T_{average}} \quad (10)$$

$$SDT = \sqrt{\frac{1}{n} \sum_{i=1}^n (T_i - T_{average})^2} \quad (11)$$

3.2. Grid independence

The temperatures of the two hotspots were selected as a reference to test the mesh independence. The relative error is calculated as follows [6]:

$$e = \frac{|T_i - T_0|}{T_0} \cdot 100\% \quad (12)$$

where e is the relative error, T_0 is the temperature simulation result obtained from the reference mesh, T_i represents the temperature simulation result obtained from other meshes. The number of grids is 4.87 million in the reference mesh. Figure 3 shows the relative error of the hotspot temperature and average pressure drop at different grids number. The relative error decreases as the number of grids increases, while the trend slows when the grids number exceeds 1.69 million. Meanwhile, the average hotspot temperature tends to stabilize. Considering the calculation accuracy and the computational burden, the mesh division method of 1.69 million grids is selected. In this case, the relative errors of the chosen hotspot temperature and the average pressure drop are 0.7% and 3.5%, respectively.

3.3. Optimization of the UCMFHS

Optimization was carried out to enhance the cooling performance of the UCMFHS. The water inlet and outlet position and pin fin position are considered to optimize the UCMFHS structure. The optimization objectives are uniform flow rate distribution and small chip temperature.

3.3.1 Optimization of water inlet and outlet position

In this experiment, multiple inlets and outlets were designed to shorten the flow length. Considering that the number and arrangement of inlets and outlets are likely to infect the cooling performance of UCMFHS, we investigated several arrangements of water inlets and outlets. As shown in Fig. 4 (a) and (b), four inlets with two outlets and four inlets with one outlet were designed. Moreover, the arrangement with inlets closer to the center of the UCMFHS was investigated, as shown in Fig. 4 (c) and (d). The distance between the inlet and outlet in four arrangements is 20.5 mm in Fig. 4 (a), 24 mm in Fig. 4 (b), 12.5 mm in Fig. 4 (c), and 17.7 mm in Fig. 4 (d) respectively. Figure 4 (e)~(h) shows the flow rate distribution under different inlets and outlets arrangements. A significantly low flow rate occurred in region A1 compared to the other regions. When the inlets got closer to the center of the UCMFHS, the flow rate decreased in the region (A2, A3) far from the center of the UCMFHS. These non-uniform flow rate distributions ultimately resulted in uneven cooling performance across multiple hotspots. Therefore, two outlets with four inlets far from the center of the UCMFHS were designed for better cooling performance. The later optimizations were conducted under these inlets and outlets positions.

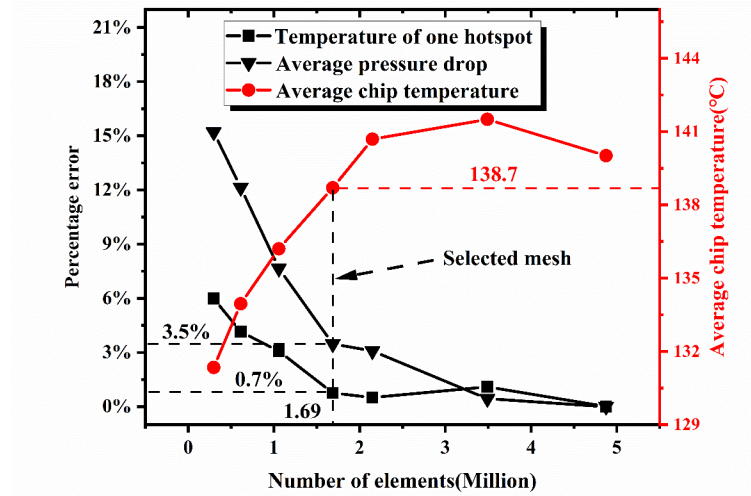


Fig. 3. Grid independence test

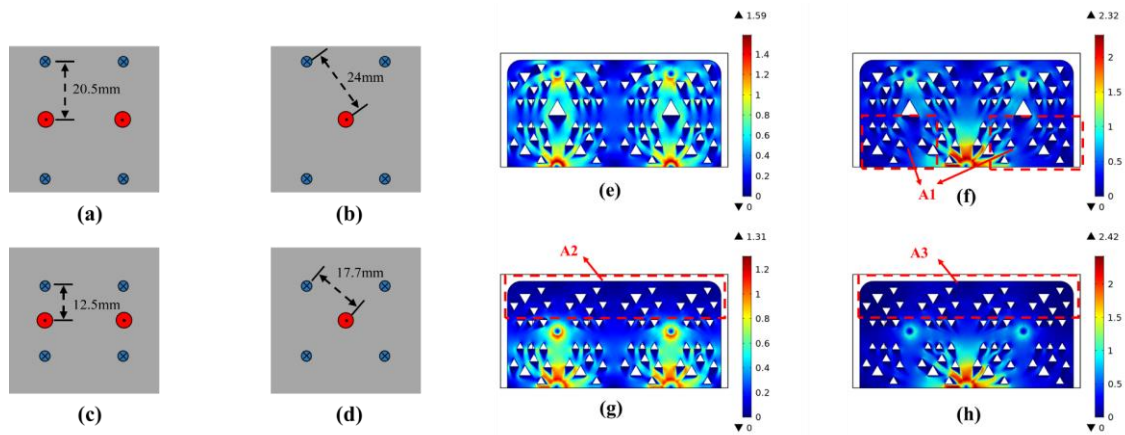


Fig. 4. The arrangement of the water inlet and outlet (a) Case 1, four inlets with two outlets; (b) Case 2, four inlets with one outlet; (c) Case 3, two outlets with inlets closer to the center of the

UCMFHS; (d) Case 4, one outlet with inlets closer to the center of the UCMFHS; The flow rate distribution under different inlet and outlet designs (e) Case1; (f) Case2; (g) Case3; (h) Case4

3.3.2 Optimization on pin fins positions

The different pin fins positions are likely to affect the flow rate distribution. So, we investigated the uniform pin fin array arrangement, which was set as the baseline, and two adjusted arrangements. Figure 5 shows the flow rate distribution under different pin fins positions. In the baseline, the flow is mainly concentrated in the region between the liquid inlet and the liquid outlet, which causes a low flow rate and high local hotspot temperature in the edge region of the UCMFHS. To obtain a more uniform flow rate distribution, the pin fins were placed in a position where they directed the fluid to a place far from the main stream. The flow in Region B was enhanced after the adjustment which allowed for a more uniform overall flow. Meanwhile, the adjusted arrangement 2 had a better enhancement effect in Region B. So, the pin fins position in adjusted arrangement 2 was adopted. The critical sizes of the optimized UCMFHS are shown in Table 1.

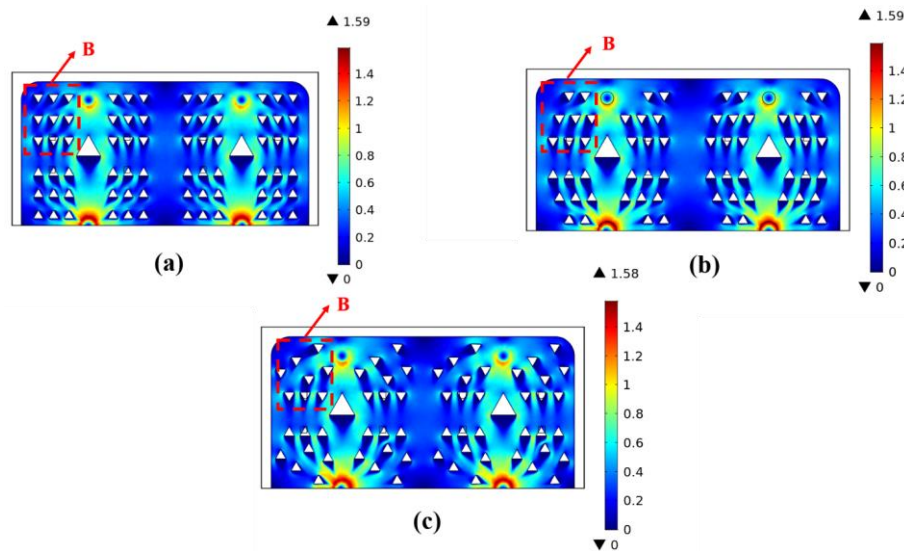


Fig. 5. The flow rate distribution under different pin fins positions. (a) Uniform array arrangement; (b) Adjusted arrangement 1; (c) Adjusted arrangement 2

Table 1. Critical size parameter of the heat sink

$a_1(\text{mm})$	$a_2(\text{mm})$	$a_3(\text{mm})$	$a_4(\text{mm})$	$a_5(\text{mm})$	$s_1(\text{mm})$
2.3	0.87	1.08	1.63	1.1	1.76
$s_2(\text{mm})$	$s_3(\text{mm})$	$s_4(\text{mm})$	$R_1(\text{mm})$	$W_1(\text{mm})$	$W_2(\text{mm})$
1.58	2.6	3.95	3	47	50

4. Experiment setup

The optimized UCMFHS was fabricated by deep reactive ion etching (DRIE) and a silicon-silicon bonding process. Then the thermal test vehicle was assembled. As shown in Fig. 6, the thermal test vehicle consists of a heat source, UCMFHS and water supply structure. To simulate the

thermal conditions of multiple hotspots microelectronic systems, the 16 TTCs were adopted as heat source arrays which were bonded to the UCMFHS by silver paste, as shown in the top view of Fig. 6.

Figure 7 shows the configuration schematic diagram and the experimental platform of the test system. The test system mainly includes test samples, a DC power supply, a differential pressure meter, a coolant reservoir, an infusion pump, an infrared camera, and a recording device. All the components were connected through plastic tubes and fittings. The TTCs were driven by two DC power supplies. And the deionized water was circulated throughout the cooling system by the infusion pump and was collected in a coolant reservoir. The temperature of the hotspots on the test samples was measured by an infrared camera and the recorded data was saved by a recording device.

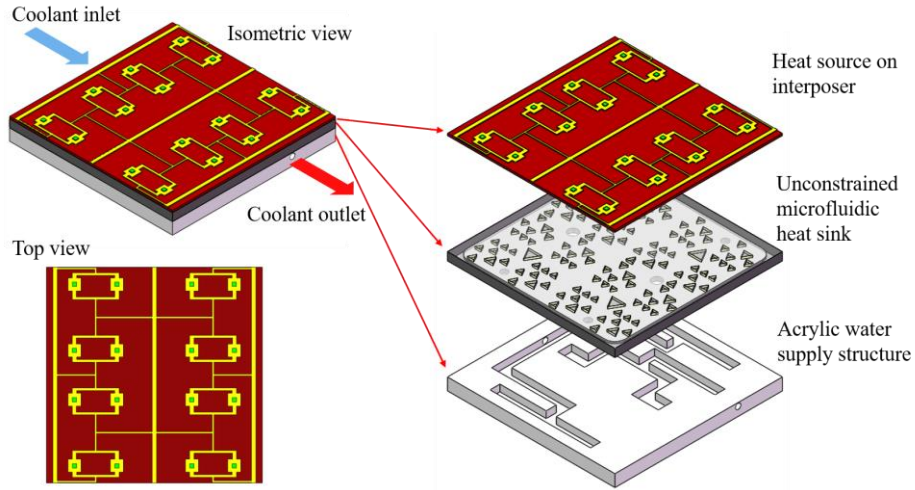


Fig. 6. Schematic diagram of the thermal test vehicle configuration

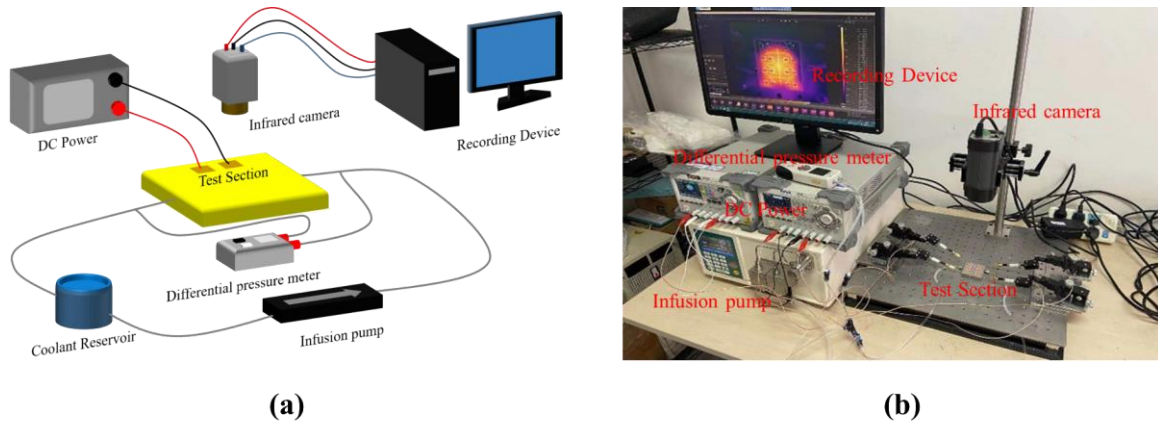


Fig. 7. (a)Schematic diagram (b) The experimental platform of the test system

5. Result and discussion

5.1 Evaluation of the anti-blockage capacity

The coolant with a mass fraction of 0.5% CuO particles, which consisted of 400 mL deionized water and 2 g CuO powder, was used to evaluate the anti-blockage capacity of the UCMFHS. Referring to the size of the filter [38], the 10 μm CuO particles were chosen. The micro pin fins microfluidic structure with a lateral fin spacing of 125 μm and a longitudinal fin spacing of 250 μm

was selected as a control sample. Figure 8 illustrates the variation of the pressure drop with time when the coolant contains particles. The particles deposited in the microfluidic structure as time flowed, causing the blockage in the microfluidic structure. The pressure drop increased at the same time. When the cooling system ran for 12 minutes, a large number of particles accumulated at the entrance of the microfluidic in the control sample, which caused the increase of pressure drop by 29.5 kPa. Then at 30 minutes, the blockage got worse in the control sample owing to the further accumulation of particles, which caused the increase of the pressure drop by 53.5 kPa. As for the unconstrained microfluidic structure, the increment of the pressure drop was less than 0.3 kPa, which is 99.43% lower than the control sample. It means that there was nearly no blockage in the unconstrained microfluidic structure. The mentioned result above shows that the UCMFHS has good anti-blockage capacity. During long-term operation, the UCMFHS can work normally even though there are particles in the coolant, indicating that the UCMFHS is highly robust.

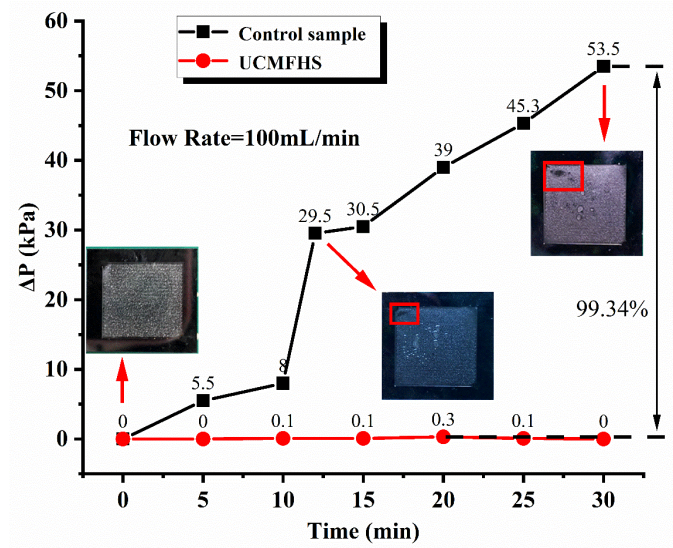


Fig. 8. The variation of the pressure drops when the coolant contains CuO particles in the control sample and UCMFHS at a flow rate of 100 mL/min

5.2. Evaluation of the thermal performance

The hotspot temperature and hotspot temperature uniformity were tested to evaluate the cooling capacity of the UCMFHS. The deionized water was selected as coolant and the water temperature was kept at 20 °C. Figure 9 (a) shows the temperature distribution of 16 hotspots at chip heat flux 1200 W/cm² and flow rate 125 mL/min. The average hotspots temperature and hotspots temperature non-uniformity coefficient were calculated to be 141.1 °C and 0.049 respectively by equation (9), (11). The chip temperatures are below the maximum tolerance of junction temperature (225 °C) [3], which indicates that the UCMFHS can be implemented for the cooling of radio frequency (RF) systems. The unconstrained microfluidic structure is symmetrical, so the temperature distribution should be symmetrical if the liquid supply is uniform. But it can be seen in Fig. 9 (a) that temperature distribution is asymmetrical. The symmetrical liquid supply structure was adopted to reduce the influence of the coolant distribution on temperature uniformity. Through further analysis, the uneven thickness of the interface material or the defects [39] in the material, which increase the interfacial thermal resistance between TTCs and UCMFHS, is thought to be the main reasons causing higher

local temperatures of some hotspots and higher temperature non-uniformity.

Figure 9 (b) shows the absolute percentage error of the simulation and experimental results of the hotspots temperature at heat flux 1200 W/cm^2 and flow rate 125 mL/min . Under such operating conditions, the average hotspots temperature and hotspots temperature non-uniformity coefficient of the UCMFHS are $141.1 \text{ }^\circ\text{C}$ and 0.049 in the experiment and $139.9 \text{ }^\circ\text{C}$ and 0.031 in the simulation. The average and maximum errors of the hotspot temperatures were 3.84% and 9.36% between the simulation and experimental results. Therefore, it can be considered that the fabricated UCMFHS conforms to the design.

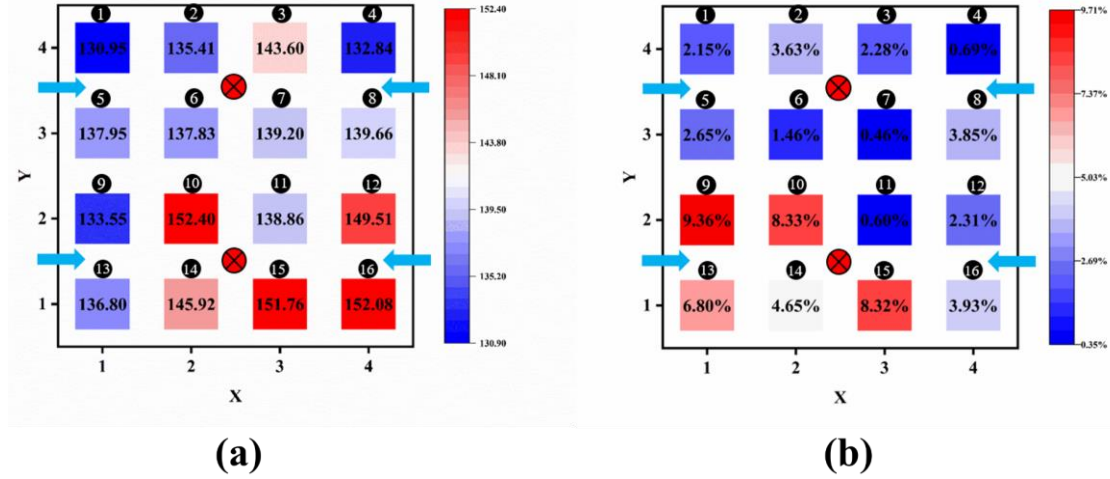


Fig. 9. (a) Temperature distribution of 16 hotspots system at a heat flux of 1200 W/cm^2 and flow rate of 125 mL/min ; (b) Percentage error between simulation and experimental result at a chip heat flux of 1200 W/cm^2 and flow rate of 125 mL/min

6. Conclusion

In this work, we proposed the UCMFHS with high anti-blockage capacity for multiple hotspot systems. Based on the above heat sink, the microfluidic structure was optimized to improve temperature uniformity. In addition, the anti-blockage capacity and cooling performance were verified by experiment. The main research results are as follows:

- The arrangement of pin fins which direct the fluid to the place far from the main stream is beneficial for temperature uniformity.
- The average 16 hotspots temperature and hotspots temperature non-uniformity coefficient were $141.1 \text{ }^\circ\text{C}$ and 0.049 respectively at chip heat flux 1200 W/cm^2 and flow rate 125 mL/min .
- The average and maximum errors between the simulation and experiment results were 3.84% and 9.36% respectively.
- The UCMFHS has good anti-blockage capacity compared to the control sample when there were 0.5% CuO particles in the coolant.

The UCMFHS has good temperature uniformity when it is used for the 16 hotspots cooling. In addition, the UCMFHS has high anti-blockage capacity, which can ensure the anti-blockage capacity in long-term operation. Therefore, the UCMFHS may be a promising option for cooling long-term operation multiple hotspots system.

Acknowledgment

This work was supported by the National Key R&D Program of China (grant number 2020YFB2008900). We also thank Suzhou Rich Sensor Science & Technology Co., Ltd for providing the thermal test chip and technical support.

Nomenclature

a_{1-5}	gap size, [mm]	u	fluid velocity, [m/s]
c_p	specific heat, [Jkg ⁻¹ K ⁻¹]	W_1	width of microfluidic, [mm]
e	relative error	W_2	width of the heat sink, [mm]
k	thermal conductivity, [Wm ⁻¹ K ⁻¹]		
p	pressure, [Pa]	<i>Greek symbols</i>	
Q	heat source, [W]	ρ	fluid density [kgm ⁻³]
R_1	corner radius, [mm]	μ	dynamic viscosity
Re	Reynolds number		
s_{1-4}	pin fins length, [mm]	<i>Acronyms</i>	
T	Temperature, [K]	NUC	non-uniformity coefficient
$T_{average}$	average hotpots temperature, [K]	SDT	standard deviation of temperature

References

- [1] Bar-Cohen, A., *et al.*, DARPA's Intra/Interchip Enhanced Cooling (ICECool) Program, *Proceedings, 27th International Conference on Compound Semiconductor Manufacturing Technology (CSMANTECH)*, New Orleans, USA, 2013, pp. 171-174
- [2] He, Z. Q., *et al.*, Thermal Management and Temperature Uniformity Enhancement of Electronic Devices by Micro Heat Sinks: A Review, *Energy*, 216 (2021), p. 119223
- [3] Iwe, H., *et al.*, Packaging and Cooling of an X-band Digital Array Radar T/R Module, *Proceedings, IEEE Radar Conference (RadarConf)*, Seattle, USA, 2017, pp. 1651-1656
- [4] Anandan, S. S., Ramalingam, V., Thermal Management of Electronics: A Review of Literature, *Thermal Science*, 12 (2008), pp. 5-26
- [5] Tuckerman, D. B., Pease, R. F. W., High-Performance Heat Sinking for VLSI, *IEEE Electron Device Letters*, 2 (1981), pp. 126-129
- [6] Zhang, D. W., *et al.*, Investigation on the Heat Transfer and Energy-saving Performance of Microfluidic with Cavities and Extended Surface, *International Journal of Heat and Mass Transfer*, 189 (2022), p. 122712
- [7] Koo, J. M., *et al.*, Integrated Microfluidic Cooling for Three-dimensional Electronic Circuit

- Architectures, *Journal of Heat Transfer*, 127 (2005), pp. 49-58
- [8] Refaey, H. A., *et al.*, Cooling Enhancement of Cubical Shapes Electronic Components Array Including Dummy Elements Inside a Rectangular Duct, *Thermal Science*, 27 (2023), pp. 1529-1538
- [9] Sekar, D., *et al.*, A 3D-IC Technology with Integrated Microfluidic Cooling, *Proceedings*, International Interconnect Technology Conference (IITC), Burlingame, USA, 2008, pp. 13-15
- [10] Cui, M. M., Song, R., Comprehensive Performance Investigation and Optimization of a Plate Fin Heat Exchanger with Wavy Fins, *Thermal Science*, 26 (2022), pp. 2261-2273
- [11] Sung, M. K., Mudawar, I., Experimental and Numerical Investigation of Single-phase Heat Transfer Using a Hybrid Jet-impingement/Micro-channel Cooling Scheme, *International Journal of Heat and Mass Transfer*, 49 (2006), pp. 682-694
- [12] Abdelmohimen, M. A. H., Numerical Investigation of Using Different Arrangement of Fin Slides on the Plate-fin Heat Sink Performance, *Thermal Science*, 25 (2021), pp. 4683-4693
- [13] Erp, R. V., *et al.*, Embedded Microfluidic Cooling for High Power-Density GaN-on-Si Power Integrated Circuits, *Proceedings*, 19th IEEE Intersociety Conference on Thermal and Thermomechanical Phenomena in Electronic Systems (ITherm), Orlando, USA, 2020, pp. 53-59
- [14] Wei, X. J., *et al.*, Experimental and Numerical Study of a Stacked Microfluidic Heat Sink for Liquid Cooling of Microelectronic Devices, *Journal of Heat Transfer*, 129 (2007), pp. 1432-1444
- [15] Gudipaty, T., *et al.*, Cluster Formation and Growth in Microfluidic Flow of Dilute Particle Suspensions, *Microfluidics and Nanofluidics*, 10 (2011), pp. 661-669
- [16] Dressaire, E., Sauret, A., Clogging of Microfluidic Systems, *Soft Matter*, 13 (2017), pp. 37-48
- [17] Agbangla, G. C., *et al.*, Experimental Investigation of Pore Clogging by Microparticles: Evidence for a Critical Flux Density of Particle Yielding Arches and Deposits, *Separation and Purification Technology*, 101 (2012), pp. 42-48
- [18] Yamaguchi, E., Adrian, R. J., Theoretical and Experimental Study of Microfluidic Blockage Phenomena, *Proceedings*, 1st ASME International Conference on Microfluidics and Minichannels, Rochester, USA, 2003, pp. 851-857
- [19] Mays, D. C., Hunt, J. R., Hydrodynamic Aspects of Particle Clogging in Porous Media, *Environmental Science & Technology*, 39 (2005), pp. 577-584
- [20] Kadam, S. T., Kumar, R., Twenty First Century Cooling Solution: Microfluidic Heat Sinks, *International Journal of Thermal Science*, 85 (2014), pp. 73-92
- [21] Pan, M. Q., *et al.*, An Investigation of Blockage Conditions on the Laminated-sheet Microfluidic Reactor, *Chemical Engineering and Technology*, 40 (2017), pp. 2289-2294
- [22] Trofa, M., *et al.*, Maffettone, Numerical Simulation of Clogging in a Microfluidic with Planar Contraction, *Physics of Fluids*, 33 (2021), p. 083320
- [23] Pejman, R., *et al.*, Najafi, How to Design a Blockage-tolerant Cooling Network, *Applied Thermal Engineering*, 181 (2020), p. 115916

- [24] Pety, S. J., *et al.*, Design of Redundant Microvascular Cooling Networks for Blockage Tolerance, *Applied Thermal Engineering*, 131 (2018), pp. 965-976
- [25] Wang, X. Q., *et al.*, Thermal Characteristics of Tree-shaped Microfluidic Nets for Cooling of a Rectangular Heat Sink, *International Journal of Thermal Science*, 45 (2006), pp. 1103-1112
- [26] Wang, X. Q., *et al.*, Numerical Analysis of Blockage and Optimization of Heat Transfer Performance of Fractal-like Microfluidic Nets, *Journal of Electronic Packaging*, 128 (2006), pp. 38-45
- [27] Xu, P., *et al.*, Thermal Characteristics of Tree-shaped Microfluidic Nets with/without Loops, *International Journal of Thermal Science*, 48 (2009), pp. 2139-2147
- [28] Wu, R. K., *et al.*, A Bi-Layer Compact Thermal Model for Uniform Chip Temperature Control with Non-uniform Heat Sources by Genetic-algorithm Optimized Microfluidic Cooling, *International Journal of Thermal Science*, 136 (2019), pp. 337-346
- [29] Riera, S., *et al.*, Stepwise Varying Width Microfluidic Cooling Device for Uniform Wall Temperature: Experimental and Numerical Study, *Applied Thermal Engineering*, 78 (2015), pp. 30-38
- [30] Ansari, D., Kim, K. Y., Hotspot Thermal Management Using a Microfluidic-pinfin Hybrid Heat Sink, *International Journal of Thermal Science*, 134 (2018), pp. 27-39
- [31] Tan, H., *et al.*, Temperature Uniformity in Convective Leaf Vein-shaped Fluid Microfluidics for Phased Array Antenna Cooling, *International Journal of Thermal science*, 150 (2020), p. 106224
- [32] Collins, L. L., *et al.*, A Permeable-membrane Microfluidic Heat Sink Made by Additive Manufacturing, *International Journal of Heat and Mass Transfer*, 131 (2019), pp. 1174-1183
- [33] Wang, Y. Y., *et al.*, Convective Heat Transfer and Mixing Enhancement in a Microfluidic with a Pillar, *International Journal of Heat and Mass Transfer*, 62 (2013), pp. 553-561
- [34] Vasilev, M. P., *et al.*, Effect of Circular Pin-fins Geometry and Their Arrangement on Heat Transfer Performance for Laminar Flow in Microfluidic Heat Sink, *International Journal of Thermal Science*, 170 (2021), p. 107177
- [35] Qu, W. L., Mudawar, I., Experimental and Numerical Study of Pressure Drop and Heat Transfer in a Single-phase Micro-channel Heat Sink, *International Journal of Heat and Mass Transfer*, 45 (2002), pp. 2549-2565
- [36] Zhang, N., *et al.*, Embedded Cooling Method with Configurability and Replaceability for Multi-chip Electronic Devices, *Energy Conversion and Management*, 253 (2022), p. 115124
- [37] Cong, B., *et al.*, Investigation on the Heat Dissipation of High Heat Flux Chip Array by Fractal Microchannel Networks, *Thermal Science*, 27(2023), pp. 869-880
- [38] Yang, M., *et al.*, Experimental Study on Single-phase Hybrid Microfluidic Cooling Using HFE-7100 for Liquid-cooled Chips, *International Journal of Heat and Mass Transfer*, 160 (2020), p. 120230
- [39] Won, Y., *et al.*, Fundamental Cooling Limits for High Power Density Gallium Nitride Electronics,

IEEE Transactions on Components, Packaging and Manufacturing Technology, 5 (2015), pp. 737-744

Received: 14.02.2023.

Revised: 25.05.2023.

Accepted: 14.07.2023